

Lattice QCD noise reduction for bosonic correlators through Blocking

Luis Altenkort,¹ Alexander M. Eller,² O. Kaczmarek,¹ Lukas Mazur,³ Guy D. Moore,² and H.-T. Shu⁴

¹*Fakultät für Physik, Universität Bielefeld, D-33615 Bielefeld, Germany*

²*Institut für Kernphysik, Technische Universität Darmstadt*

Schlossgartenstraße 2, D-64289 Darmstadt, Germany

³*Paderborn Center for Parallel Computing, Paderborn University, D-33098 Paderborn, Germany*

⁴*Institut für Theoretische Physik, Universität Regensburg, D-93040 Regensburg, Germany.*

We propose a method to substantially improve the signal-to-noise ratio of lattice correlation functions for bosonic operators or other operator combinations with disconnected contributions. The technique is applicable for correlations between operators on two planes (zero momentum correlators) when the dimension of the plane is larger than the separation between the two planes which are correlated. In this case, the correlation arises primarily from points whose in-plane coordinates are close; but noise arises from all pairs of points. By breaking each plane into bins and computing bin-bin correlations, it is possible to capture these short-distance correlators exactly while replacing (small) correlators at large space extent with a fit, with smaller uncertainty than the data. The cost is only marginally larger than averaging each plane before correlating, but the improvement in signal-to-noise can be substantial. We test the method on correlators of the gradient-flowed topological density and squared field strength, finding noise reductions by $\sim 3 - 7$ compared to the conventional approach on the same ensemble of configurations.

I. INTRODUCTION

Many problems in quantum field theory can be expressed in terms of the correlation function of two operators as a function of separation along one axis, while averaging over directions transverse to that axis. For example, when the operators are the interpolating operator for a particle, the exponential rate of the falloff of the correlator determines the particle mass. Moreover, zero spatial-momentum correlators of conserved currents, such as the energy-momentum tensor (EMT) or the vector current, encode transport coefficients like shear and bulk viscosity or flavor diffusion coefficients and the electrical conductivity in the small-frequency limiting behavior of their reconstructed spectral functions. For a review see [1]. Some recent lattice studies using this approach for the calculation of viscosities can be found in [2–6] and for a recent overview of results for the electrical conductivity see [7]. Problems like these ultimately come down to the computation of correlation functions of operators averaged over a transverse plane, evaluated as a function of the separation between two planes.

Usually such studies require that the correlation function be determined very precisely. For fermionic operators which carry nontrivial flavor, this is generally not a problem; there are explicit factors of propagators between the two planes, which cause the configuration-by-configuration value of the correlator to decay. In this case the signal to noise is generally good, and the main limitations are, for example, contamination from higher states, the continuum limit, etc. However, in some cases the correlation function is very noisy due to disconnected contributions in the squared correlator, as we explain in Sec. II.

This paper will introduce and demonstrate a new approach for problems where such disconnected contributions lead to severe signal-to-noise problems. We show a

numerically efficient way to express the correlation function between operators on two planes as an integral over the transverse separation between the operator locations on the planes in Sec. III. The signal is dominated by small transverse separations; the noise is dominated by large transverse separations. By fitting the region with a strong signal and using the fit where the signal is poor, one can avoid these noisy contributions, improving the overall signal-to-noise significantly. We demonstrate this for EMT correlators in the bulk channel and topological charge density correlator in Sec. IV. As a byproduct of this work we also update the double extrapolated topological charge density correlators which we provided recently [8].

II. ORIGIN OF THE PROBLEM

Consider an operator \mathcal{O} of dimension Δ and its Hermitian conjugate \mathcal{O}^\dagger . Suppose we are interested in the correlation function

$$G(\tau) \equiv \int d\vec{x}d\vec{y} \langle \mathcal{O}^\dagger(\vec{x}, \tau) \mathcal{O}(\vec{y}, 0) \rangle. \quad (1)$$

Here the transverse space integration $d\vec{x}$ is over a transverse space of extent L^3 , and we are primarily concerned with the case where $\tau \ll L$. This is the case for transport coefficients because $\tau < 1/(2T)$ but $L \gg 1/T$ to ensure that we are close to the thermodynamic limit. In the opposite limit, that is $\tau > L$, our approach will be ineffective. For correlations between planes which include the time direction and are separated instead along a space axis, exchange the label τ for the label of the relevant space direction in what follows.

First let us analyze the expected size of the signal. On

dimensional grounds we expect that

$$\begin{aligned} \langle \mathcal{O}^\dagger(\vec{x}, \tau) \mathcal{O}(\vec{y}, 0) \rangle &\sim ((\vec{x} - \vec{y})^2 + \tau^2)^{-\Delta}, \\ G(\tau) &= \int d^3\vec{y} \langle \mathcal{O}^\dagger(\vec{x}, \tau) \mathcal{O}(\vec{y}, 0) \rangle \\ &\propto \int d^3\frac{\vec{x} + \vec{y}}{2} \int d^3(\vec{x} - \vec{y}) \frac{1}{((\vec{x} - \vec{y})^2 + \tau^2)^\Delta} \\ &\sim L^3 \tau^{3-2\Delta}. \end{aligned} \quad (2)$$

The correlation function is extensive in the transverse area because of the integral over the average coordinate

$(\vec{x} + \vec{y})/2$; the integral over the difference coordinate $\vec{x} - \vec{y}$ is dominated by $|\vec{x} - \vec{y}| \lesssim \tau$.

If a large mass gap plays a role in the correlator of interest, the decay will instead be exponential. In general, one expects polynomial decay at short distances and exponential decay at large distances.

Next we want to understand the noise. The signal-to-noise achieved from N_{sample} independent gauge field configurations will scale as $1/\sqrt{N_{\text{sample}}}$ times the signal-to-noise from a single configuration. We can estimate this noise by asking about the mean value of $G(\tau)$ and about the mean-squared value of $G(\tau)$. Then the variance of the measurement is determined as usual by:

$$\begin{aligned} \sigma_G^2 &= \langle G(\tau) G^*(\tau) \rangle - |\langle G(\tau) \rangle|^2 \\ &= \int d\vec{x}_1 d\vec{x}_2 d\vec{y}_1 d\vec{y}_2 (\langle \mathcal{O}^\dagger(\vec{x}_1, \tau) \mathcal{O}(\vec{x}_2, \tau) \mathcal{O}(\vec{y}_1, 0) \mathcal{O}^\dagger(\vec{y}_2, 0) \rangle - \langle \mathcal{O}^\dagger(\vec{x}_1, \tau) \mathcal{O}(\vec{y}_1, 0) \rangle \langle \mathcal{O}(\vec{x}_2, \tau) \mathcal{O}^\dagger(\vec{y}_2, 0) \rangle) \\ &\simeq \int d\vec{x}_1 d\vec{x}_2 \langle \mathcal{O}^\dagger(\vec{x}_1, \tau) \mathcal{O}(\vec{x}_2, \tau) \rangle \int d\vec{y}_1 d\vec{y}_2 \langle \mathcal{O}(\vec{y}_1, 0) \mathcal{O}^\dagger(\vec{y}_2, 0) \rangle \\ &\sim \int d^3\frac{\vec{x}_1 + \vec{x}_2}{2} \int d^3(\vec{x}_1 - \vec{x}_2) |\vec{x}_1 - \vec{x}_2|^{-2\Delta} \int d^3\frac{\vec{y}_1 + \vec{y}_2}{2} \int d^3(\vec{y}_1 - \vec{y}_2) |\vec{y}_1 - \vec{y}_2|^{-2\Delta}. \end{aligned} \quad (3)$$

The first term in the second line is the *full* correlator, including both the connected correlator and various disconnected contributions. We assume that the variance is dominated by the disconnected contribution of this term which appears in the third line, since this contribution receives large small-separation contributions when $\vec{x}_1 \approx \vec{x}_2$ and $\vec{y}_1 \approx \vec{y}_2$.

The variance has two worrying features. First, the integrals over $(\vec{x}_1 - \vec{x}_2)$ and $(\vec{y}_1 - \vec{y}_2)$ are short-distance divergent, presumably cut off by the lattice spacing a . Second, each overall integration $\int d^3(\vec{x}_1 + \vec{x}_2)/2$, $\int d^3(\vec{y}_1 + \vec{y}_2)/2$ introduces an overall L^3 factor. Thus one estimates that

$$\sigma_G^2 \sim L^6 a^{6-4\Delta}. \quad (4)$$

The signal-to-noise from correlating a single pair of planes on a single lattice is therefore on the order of $G(\tau)/\sigma_G \sim (a/\tau)^{2\Delta-3} \ll 1$.

The gradient flow method [9, 10] offers an approach to ameliorate the short-distance divergent behavior in these correlation functions. Rather than evaluating the correlation functions directly on the lattice configuration, one first applies a well-defined procedure to remove UV fluctuations in the fields down to a length scale $\sim \sqrt{8\tau_F}$, with τ_F the gradient-flow depth. This reduces the divergent short-distance behavior such that $\int d\vec{x} \langle \mathcal{O}^\dagger(\vec{x}, 0) \mathcal{O}(\vec{0}, 0) \rangle \sim (8t)^{(3-\Delta)/2}$. Physical results require an extrapolation to small t , which partially counteracts the gain in signal-to-noise. Nevertheless, it is still necessary to apply some additional kind of noise reduction technique in order to get a signal in a reasonable

amount of computing time.¹

This leaves, however, the problem that the signal-to-noise does not improve as one makes L large. One might have hoped for such improvement, because boxes with larger transverse extent L should be generating more statistically independent samples. But we do not see such an improvement in our parametric estimates, nor in simulations. To see why, we look at the role of transverse integrations in the signal and in the noise. In Eq. (2) we see that only $|\vec{x} - \vec{y}| \lesssim \tau$, that is, small transverse separations, contribute to the signal. But Eq. (3) contains *independent* integrations over $d\vec{x}$ and $d\vec{y}$; all values of $\vec{x} - \vec{y}$ contribute equally to the noise. So points with small transverse difference are responsible for signal and noise; but points with large transverse difference contribute to the noise, but not to the signal.

In this work we propose a blocking technique which eliminates the noise contributions from large transverse separations, and restores the expected behavior that the signal-to-noise ratio improves as $(L/\tau)^{3/2}$. The technique

¹ An alternative noise-reduction technique is the use of the multi-level algorithm [11]. The multilevel method has been successfully applied to correlation functions relevant for transport [12–15]. However, this technique is only applicable to pure-gauge theories; it cannot directly be generalized to the unquenched case. Furthermore, it is implemented using Monte Carlo updates of the gauge fields, rather than during the calculation of correlation functions on generated configurations. Ideas on the implementation of multilevel algorithms including dynamical fermions can be found in [16, 17].

is numerically cheap and can be used in conjunction with gradient flow. In addition, it is applied at the analysis level, not as part of the configuration generation, and it is perfectly compatible with unquenching.

Naturally we are far from the first people to confront this particular problem. The issue of rapid falloff in the signal but not the noise has been known for a long time [18], and has been discussed and confronted frequently in the recent literature [19–23]. In particular, Ref. [24] present an approach which is in some ways similar to what we argue for here. We will discuss the relative advantages of the approaches after giving an exposition of what we propose.

III. BLOCKING METHOD

Let us specialize to Hermitian operators \mathcal{O} and consider the lattice form of the correlation function, where space integrals are replaced by discrete sums:

$$G(\tau_1 - \tau_2) = \frac{1}{V} \sum_{\vec{x} \in V} \mathcal{O}(\tau_1, \vec{x}) \sum_{\vec{y} \in V} \mathcal{O}(\tau_2, \vec{y}), \quad (5)$$

where $V = N_x N_y N_z$ is the spatial volume of the lattice. To calculate it one first evaluates the operator on each site on the plane at temporal position τ_1 and also those at τ_2 . The two planes are shown as grey squares at $\tau = \tau_1$ and $\tau = \tau_2$ in a simplified 3D sketch in Fig. 1. Then one calculates all site-to-site correlators of two operators: one operator runs over all sites on plane $\tau = \tau_1$ while the other is fixed to one site on plane $\tau = \tau_2$ and the process is repeated for each site on the second plane. The economical and also the most common way to do this is to first compute the sum of the operators on the plane at $\tau = \tau_1$ and then repeat this procedure for all planes. The data on each plane can be reduced to a single number, thus saving memory.

The method mentioned above includes contributions from all possible spatial distances ($s = \sqrt{(\vec{x} - \vec{y})^2}$). But as we have seen, the signal is dominated by small $s \lesssim \tau_2 - \tau_1$. Therefore, we want to obtain differential information, namely, how the correlation function varies as a function of s . A complete differential measurement involves correlating each \vec{x} position with each \vec{y} position. The numerical cost of this scales as V^2 , which is prohibitive, so we must seek a numerically less costly alternative, which we now present.

In the blocking method, each plane, for instance the $\tau = \tau_1$ plane in Fig. 1, is split into equal-sized bins. In each bin, we measure the operator on all sites belonging to this bin and save the sum at one corner. For instance, the blue square in Fig. 1 encloses one bin of size 2×2 and the sum is denoted as a dot at the origin. The relative position of this dot inside of the bin should be the same for all bins. Covering the whole lattice with bins leads to Fig. 2, in which the original lattice has effectively been compressed into a smaller lattice denoted by the blue

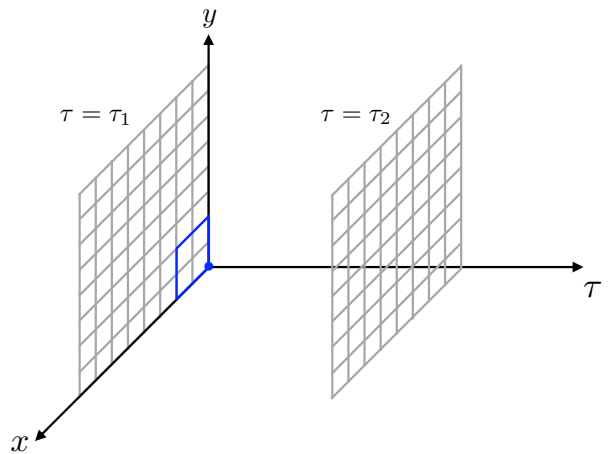


FIG. 1. Illustration of a 3-d lattice on which a temporal correlator is measured. Operators at each site of plane $\tau = \tau_1$ are summed and the same is done for $\tau = \tau_2$. Two summed operators will be correlated via Eq. (5).

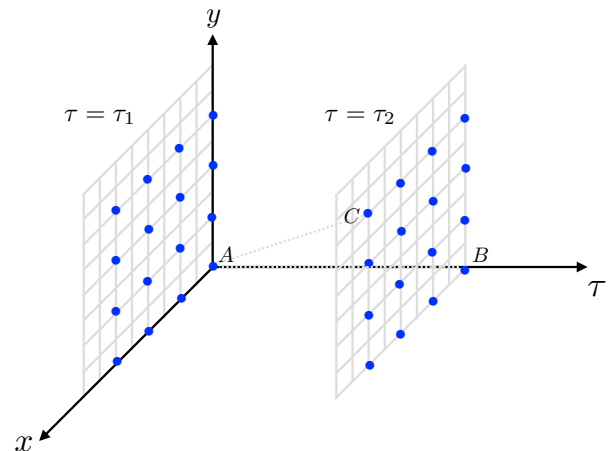


FIG. 2. Illustration of how the blocking method works: each plane is divided into bins. The operators in each bin are summed and saved to the site denoted by the blue dot on the corner. Then, for each pair of planes, one computes the correlators of all pairs of blue dots, one on each plane.

dots. On this smaller lattice a calculation of the point-to-point correlators at all possible distances is feasible. One can see this procedure is nothing but rewriting Eq. (5) as

$$G(\tau) = \frac{1}{V} \sum_{v_1 \in V} \left(\sum_{\vec{m} \in v_1} \mathcal{O}(\tau_1, \vec{m}) \right) \sum_{v_2 \in V} \left(\sum_{\vec{n} \in v_2} \mathcal{O}(\tau_2, \vec{n}) \right), \quad (6)$$

where $\tau = \tau_1 - \tau_2$, v_1, v_2 are the individual bins in each plane, and $\vec{m} \in v_1$ are all points in the bin v_1 . We advocate the use of cubic bins, that is, each bin contains

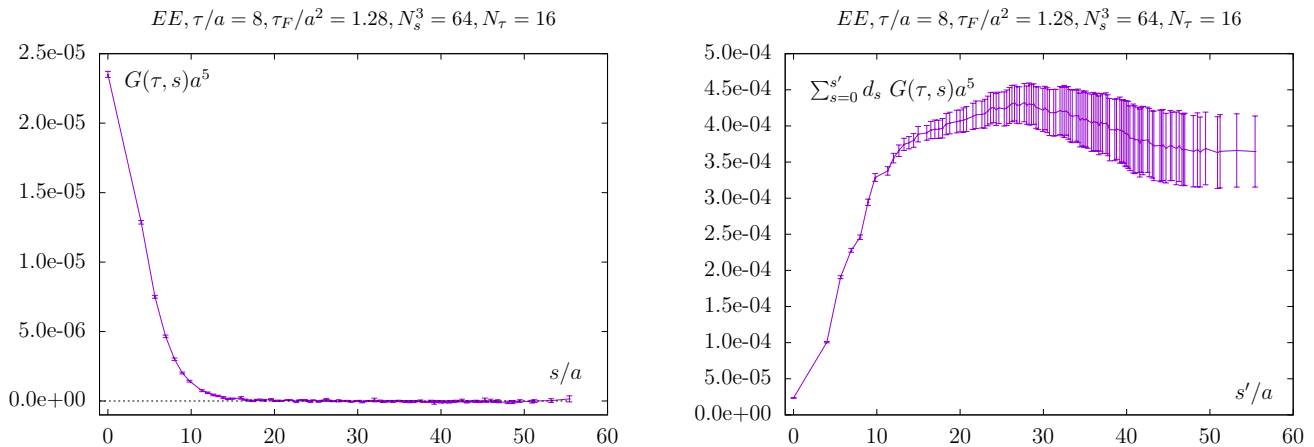


FIG. 3. *Left:* (Bare) energy-momentum tensor correlator as a function of spatial distance s on a 16×64^3 lattice at temperature $T = 1.5 T_c$ in the bulk channel at temporal separation $\tau/a = 8$ and flow depth $\tau_F/a^2 = 1.28$. The correlator is measured using the blocking method on 10000 quenched configurations. The bin size is $4 \times 4 \times 4$. *Right:* Sum of the correlator (sum of all terms $s \leq s'$) as a function of maximal spatial distance s' . The last data point (at the largest s') is equal to the correlator calculated in the conventional way (without blocking) using Eq. (5).

$V_b = n_b \times n_b \times n_b$ lattice sites. Defining

$$\begin{aligned} \mathcal{O}_{v_1}(\tau_1) &= \sum_{\vec{m} \in v_1} \mathcal{O}(\tau_1, \vec{m}) \\ G_{v_1 v_2}(\tau) &= \langle \mathcal{O}_{v_1}(\tau_1) \mathcal{O}_{v_2}(\tau_2) \rangle \end{aligned} \quad (7)$$

we can re-express Eq. (6) as

$$G(\tau) = \frac{1}{V} \sum_{v_1, v_2} G_{v_1 v_2}(\tau). \quad (8)$$

It is useful to rearrange this sum in terms of the transverse separation between the corner points of the bins $s = |\vec{v}_1 - \vec{v}_2|$. For $s = 0$ there are V/V_b contributions (equal to the number of bins). For any other s value there is an additional degeneracy factor d_s . For instance, for $s = n_b$ we can have $\vec{v}_1 - \vec{v}_2 \in \{[\pm n_b, 0, 0], [0, \pm n_b, 0], [0, 0, \pm n_b]\}$ for a total of $d_s = 6$ degenerate choices.² Introducing the sum of all correlations between bins with separation s , normalized to contain V/V_d contributions,

$$G(\tau, s) = d_s^{-1} \sum_{v_1, v_2} G_{v_1 v_2}(\tau) \delta(|\vec{v}_1 - \vec{v}_2| - s), \quad (9)$$

we can write the total correlation function as

$$G(\tau) = \frac{1}{V_b} \sum_s d_s G(\tau, s). \quad (10)$$

This representation will be particularly practical in the following. Specifically, $G(\tau, s)$ should be a smooth function of s , which allows us to fit its behavior in a range of

s where the signal-to-noise is good, and to use this fit to estimate its behavior at large s , where the signal-to-noise is bad.

A similar decomposition can be achieved using Fourier techniques, as described in Ref. [24]. To get something analogous to Eq. (9), one could sum the resulting separation-by-separation correlator into a histogram. But our main differences from the approach of Ref. [24] will be in how we use this differential information. The next section will show how we extract the integrated correlator, applying it to two specific physical problems.

IV. APPLICATIONS OF THE BLOCKING METHOD

Let us illustrate how to take advantage of blocked-correlator information in a real calculation which can be used to study transport phenomena.

Bulk viscosity can be determined from the small-frequency behavior of the spectral function for the squared field strength operator

$$E(x) = \frac{1}{4} F_{\rho\sigma}^a(x) F_{\rho\sigma}^a(x). \quad (11)$$

To compute bulk viscosity on the lattice, we first need the zero-momentum correlation function

$$G(\tau) \equiv \int d\vec{x} \langle \delta E(0, \vec{0}) \delta E(\tau, \vec{x}) \rangle \quad (12)$$

as a function of τ . Here $\delta E(x) \equiv E(x) - \langle E(x) \rangle$ is the field strength with its expectation value subtracted off to remove the disconnected contributions. In our implementation, we construct E using the clover definition of the field strength tensor. In this work we will focus

² Normalizing s to $s^2/n_b^2 = 0, 1, 2, 3, \dots$, the d_s with $s^2 \leq (L/2n_b)^2$ are the OEIS integer sequence A005875, see <https://oeis.org/A005875>

on determining this correlator with good signal-to-noise. The issues of correctly normalizing the operator, continuum and zero-flow extrapolating, and extracting the bulk viscosity from $G(\tau)$ are left for a separate study. We measure this correlator using the blocking method on a $64^3 \times 16$ quenched lattice over 10000 configurations under gradient flow, determining errors using the bootstrap method. The bin size is $4 \times 4 \times 4$. The lattice setup and gradient flow setup are the same as used in ref. [8].

We illustrate the EMT correlators calculated using the blocking method in Fig. 3. The left panel shows the correlator $G(s, \tau)$ as a function of s at a fixed flow time $\tau_F/a^2 = 1.28$ and temporal separation $\tau/a = 8$, where a is the lattice spacing. We can see that $G(s, \tau)$ is a relatively smooth function of s , and that it falls off fast such that only the first few data points ($s \lesssim 15$) contribute significantly to its overall value. At distances $s > 17$ the correlators cannot be statistically distinguished from zero. If one sums the correlator over all $s \leq s'$, including the degeneracy factor, one obtains the data shown in the right panel of Fig. 3. The data point at the largest s' recovers the result and errors calculated in the usual (nonblocking) way. It can be seen that at $s' \sim 15$ the integrated correlator reaches a plateau but the error size becomes larger and larger as s' increases. From this it is clear that the bin-to-bin correlators with small s are contributing most of the signal while the large- s ones mainly introduce noise. The key idea of the blocking method is to use only the reliable lattice data coming from small s and to estimate the contribution from the long tail by fitting the data that has good signal-to-noise using some theoretically inspired ansatz.

For each (τ, τ_F) pair, we break the s -range into three regions based on two cut points, s_0 and s_{cut} . The first region, $s < s_0$, is characterized by very high signal-to-noise ratios in the data $G(\tau, s)$. The point s_0 is chosen as the largest s -value where the signal-to-noise is better than 10. This point is very easy to find from the data, and its value is stable across different bootstrap samples. The middle region $s_0 \leq s \leq s_{\text{cut}}$, is characterized by signal-to-noise between 10 and 2. s_{cut} is determined in a self-consistent way which we will explain soon. Finally, there is the region $s > s_{\text{cut}}$, where the signal-to-noise is very poor. Our procedure is to perform a fit of the data, and to replace a direct evaluation of $G(\tau)$ with an evaluation which takes into account the fit, as follows:

$$\begin{aligned}
 G(\tau) &= G_{\text{dom}}(\tau) + G_{\text{mid}}(\tau) + G_{\text{tail}}(\tau), \\
 G_{\text{dom}}(\tau) &\equiv \frac{1}{V_b} \sum_{s=0}^{s_0-1} d_s G(\tau, s), \\
 G_{\text{mid}}(\tau) &\equiv \frac{1}{V_b} \sum_{s=s_0}^{s_{\text{cut}}} d_s (x G_{\text{fit}}(\tau, s) + (1-x) G(\tau, s)), \\
 G_{\text{tail}}(\tau) &\equiv \frac{1}{V_b} \sum_{s>s_{\text{cut}}} d_s G_{\text{fit}}(\tau, s). \tag{13}
 \end{aligned}$$

Here $x = (s - s_0)/(s_{\text{cut}} - s_0)$ is the fraction of the way

from s_0 to s_{cut} – that is, in the first region we purely use the data, in the middle region we vary linearly from purely using the data at $s = s_0$ to purely using the fit at $s = s_{\text{cut}}$, and in the final region we purely use the fit.

To perform a fit of the data we need two things; an ansatz, and a data range to use in the fit. We will return to the ansatz momentarily. First we need to emphasize what s -range the fit needs to be precise in. It is not important to find a fit function which describes the whole s range. As we see in Eq. (13), we only use the fit for $s \geq s_0$. We know on physical grounds that $G(\tau, s)$ falls rapidly at large s , and this should be reflected in our ansatz. Therefore, the data range where $G_{\text{fit}}(\tau, s)$ is most important is the range around s_0 and s_{cut} . This fact needs to be reflected both in our choice of ansatz, and in the data range we use to fit the ansatz. In particular, using data with $s < s_0$ in our fitting procedure is actually not a good idea. The high signal-to-noise tends to control the fit, but it gives information about the functional form too far away from the region where we need the fit to work. Therefore, we choose instead to fit the data with $s \geq s_0$. We could cut off the s -range used in the fitting procedure, for instance, at the not-yet-established value s_{cut} , but in practice the fit is always dominated by the first few points above s_0 , even if we use *all* data with $s \geq s_0$. This is in fact what we do; we fit a physically well motivated ansatz to all data with $s \geq s_0$. We have checked that the fit, χ^2 , and errors in the fit parameters are almost unaffected by introducing an upper cutoff on the s -range used in the fit.

With a fit in hand, we can then estimate the signal-to-noise ratio as $\text{STN}(s) = G_{\text{fit}}(\tau, s)/\sigma(\tau, s)$, where the noise is determined from the fluctuations in the data and the signal is estimated from the fit. We choose s_{cut} to be the s -value above which this estimated signal-to-noise ratio is always worse than 2. That is, we fully replace the data with the result of our fit starting where the signal-to-noise is consistently below 2. We estimate the errors in G_{mid} and G_{tail} using the determined errors in the fit coefficients.

Next we discuss the ansatz(es) used in the fits. The choice of ansatz is clearly dependent on the specifics of the theory under consideration; here we specialize to correlation functions of the action density E and of the topological charge density q .

The first ansatz is a simple power law in s , $G(s, \tau) = A(s/s_{\text{pivot}})^{-B}$, where A and B are fit parameters and s_{pivot} is the third s -value larger than s_0 .³ This is motivated by the idea that the correlation function falls off as a power of distance, with the power containing an unknown anomalous dimension which must be fitted for.⁴

³ s_{pivot} is introduced to suppress the correlation between A and B , which stabilizes the fit.

⁴ If the falloff is with distance, one should really fit to $(s^2 + \tau^2)^{-B/2}$. Since s_{cut} is almost always significantly larger than τ , this turns out to make very little difference.

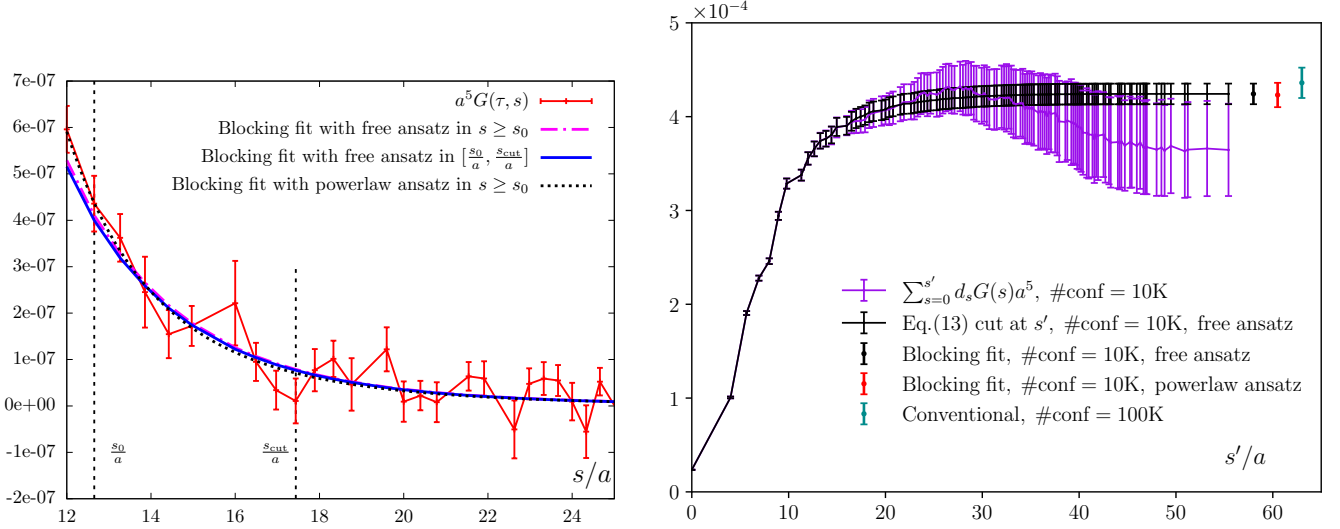


FIG. 4. *Left*: the same data as in the left panel of Fig. 3, but zoomed in around the value where the signal-to-noise becomes poor, together with three fits of the data, representing fitting functions and fit ranges as described in the text. *Right*: the same as the right plot in Fig. 3, but also showing the result summed over $s \leq s'$ using the mix of data and ansatz defined in Eq. (13). Also, the fully summed result from Eq. (13) (using powerlaw and free ansatz) and from the conventional approach using ten times as many configurations are shown (with a slight horizontal offset) as single data points on the far right.

The second ansatz is based on the leading-order perturbative value for the correlator, accounting for time-periodicity, gradient flow, and our blocking procedure. In vacuum, the leading order correlator of two field strength tensors is

$$\langle F_{\mu\nu}^a(r) F_{\alpha\beta}^b(0) \rangle = \frac{g^2 \delta_{ab}}{\pi^2 r^4} \left[\delta_{\mu\alpha} \delta_{\nu\beta} - \delta_{\mu\beta} \delta_{\nu\alpha} - \frac{2}{r^2} (r_\mu r_\alpha \delta_{\nu\beta} - r_\mu r_\beta \delta_{\nu\alpha} - r_\nu r_\alpha \delta_{\mu\beta} + r_\nu r_\beta \delta_{\mu\alpha}) \right]. \quad (14)$$

Applying gradient flow to a depth τ_F modifies this ex-

pression to:

$$\langle G_{\mu\nu}^a(r) G_{\alpha\beta}^b(0) \rangle_{\tau_F} = \frac{g^2 \delta_{ab}}{\pi^2 r^4} \left[A(r, \tau_F) (\delta_{\mu\alpha} \delta_{\nu\beta} - \delta_{\mu\beta} \delta_{\nu\alpha}) + \frac{B(r, \tau_F)}{r^2} (r_\mu r_\alpha \delta_{\nu\beta} - r_\mu r_\beta \delta_{\nu\alpha} - r_\nu r_\alpha \delta_{\mu\beta} + r_\nu r_\beta \delta_{\mu\alpha}) \right], \quad (15)$$

$$A(r, \tau_F) = 1 - \left(1 + \frac{r^2}{8\tau_F} \right) e^{-r^2/8\tau_F}, \quad (16)$$

$$B(r, \tau_F) = -2 + \left[2 - 2 \frac{r^2}{8\tau_F} + \left(\frac{r^2}{8\tau_F} \right)^2 \right] e^{-r^2/8\tau_F}. \quad (17)$$

Using these expressions, the leading-order $\langle EE \rangle$ correlator at finite $\tau_F, \tau, |\vec{r}|$ and with periodic boundaries in the time direction is

$$\langle E(\vec{r}, \tau) E(0, 0) \rangle_{\tau_F} \propto \sum_{n_1, n_2 \in \mathcal{Z}} \frac{A(r_1)A(r_2)}{r_1^4 r_2^4} + \frac{A(r_1)B(r_2) + A(r_2)B(r_1)}{2r_1^4 r_2^4} + \frac{B(r_1)B(r_2)}{6r_1^6 r_2^6} (2(r_1 \cdot r_2)^2 + r_1^2 r_2^2), \quad (18)$$

where $r_1 = (\tau + n_1 \beta, \vec{r})$ and $r_2 = (\tau + n_2 \beta, \vec{r})$ are the 4-displacement with the temporal displacement shifted by independent integer multiples of the inverse temperature β . Similarly, when we compute the correlation function of two topological density operators $q = F_{\mu\nu} \tilde{F}_{\mu\nu} / 32\pi^2$ (see below), the leading-order correlation function after flow is

$$\langle q(\vec{r}, \tau) q(0, 0) \rangle_{\tau_F} \propto - \sum_{n_1, n_2 \in \mathcal{Z}} \frac{A(r_1)A(r_2)}{r_1^4 r_2^4} + \frac{A(r_1)B(r_2) + A(r_2)B(r_1)}{2r_1^4 r_2^4} + \frac{B(r_1)B(r_2)}{6r_1^6 r_2^6} (r_1^2 r_2^2 - (r_1 \cdot r_2)^2). \quad (19)$$

Our second ansatz is, for each s -value, to integrate these expressions over the relative coordinates in the two

bins whose centers are separated by s to determine what the time-periodic, flowed, bin-averaged correlation func-

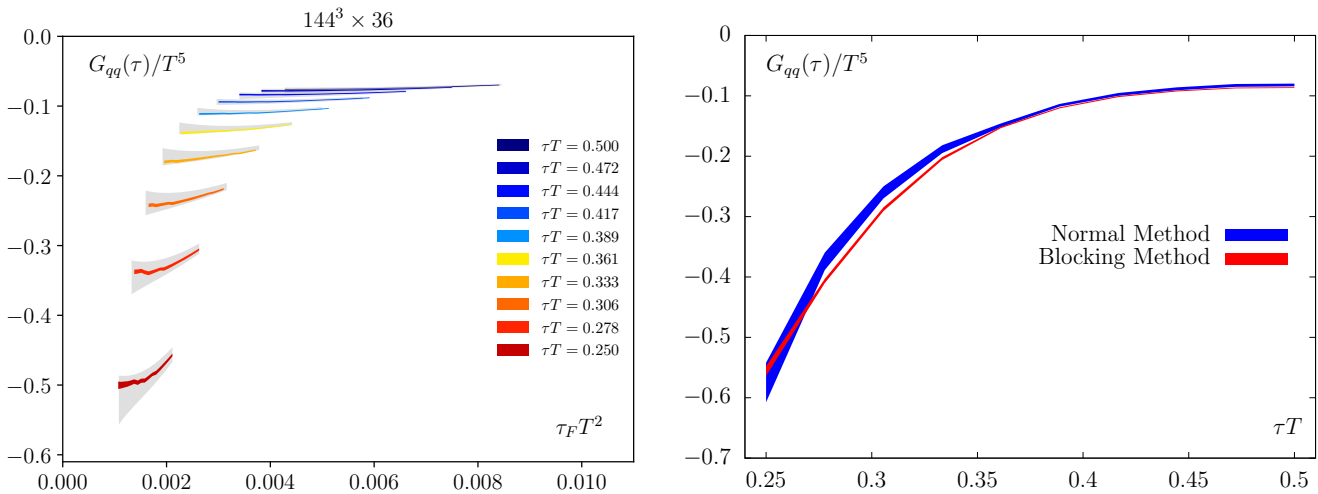


FIG. 5. Left: a comparison of the topological charge density correlators measured in the conventional way on 10000 configurations taken from [8] (grey bands) and those from blocking fits (colorful bands) on the same configurations on the $144^3 \times 36$ lattice. Right: the same as left, but after continuum and flow-time-to-zero extrapolation.

tion would be at leading perturbative order. We then fit to a single overall normalization. This fit gives a poor description of the *whole* correlator $G(s, \tau)$, because it does not get the ratio of the peak to the tail accurately. However, it gives a reasonable description of the tail shape with a single fitting parameter.

Some readers may be concerned about the ad-hoc and poorly physically motivated nature of these fitting functions. It is important to emphasize three things:

(i) The function $G(s, \tau)$ falls very fast with s . Perturbatively, $G(s, \tau) \propto s^{-8}$. We see this rapid falloff explicitly in Fig. 3, both in the data and in the fits. Therefore, it is only important that our fit to $G(s, \tau)$ be reasonable for a range above s_0 .

(ii) The fit is stable when we introduce an upper s -cutoff on the fit range, and it is stable when we adjust (somewhat) the starting point s_0 for the fit.

(iii) The influence of the fit ansatz is small, as determined by comparing these two rather different ansatz choices.

To illustrate these points, consider Fig. 4. The left panel shows the same data as in Fig. 3, but zoomed in around the region where the signal-to-noise becomes poor. The vertical bars indicate s_0 and s_{cut} , the red points are the data, and the indicated lines are three fits to the data. We see that the power-law fit and the free-ansatz fit are nearly the same, and the free-ansatz fit is almost unchanged when we fit to the data in the range $[s_0, s_{\text{cut}}]$ rather than all data with $s \geq s_0$. The fit indicates that the correlation function becomes very small for s a little higher than s_{cut} , consistent with the data but without the large error bars.

In the right panel of Fig. 4 we show a comparison of the correlators measured in the conventional way on 10000 configurations (green data point), fitted correlators based on blocking data on 10000 configurations with the free

ansatz (black points), and the same using the power-law ansatz (red data point). These are compared to the same partial sums as in Fig. 3. We can see that if we fit the tail of our data to a proper ansatz, we can reduce the error by a significant factor (in this case by a factor of ~ 4). Comparison with a much larger data set shows that this is achieved without corrupting the value; the blocking method gives a result which is consistent with that achieved by the conventional method using 10 times more data.

An alternative approach, advocated in Ref. [24], is to use physical arguments to determine the s -value where almost all of the signal has been included, and to discard the data at higher S values. In Fig. 4, this would correspond to using the purple data point at an s' value somewhere above $s' = 20$. We see that this approach would be consistent with ours, but with larger errors.

As an application of our technique, we re-analyze the topological charge density correlators which we originally explored in Ref. [8]. The correlation function under study is

$$G_{qq}(\tau) = \int d\vec{x} \langle q(\vec{0}, 0) q(\vec{x}, \tau) \rangle, \quad (20)$$

where the topological charge density is defined as

$$q(x) = \frac{g^2}{32\pi^2} \epsilon_{\mu\nu\rho\sigma} \text{Tr} \{ F_{\mu\nu}(x) F_{\rho\sigma}(x) \}. \quad (21)$$

Our implementation constructs this operator using an improved field strength tensor $F_{\mu\nu}(x)$, see [8] for details. We repeat the analysis of [8] carried out on five lattices $64^3 \times 16$, $80^3 \times 20$, $96^3 \times 24$, $120^3 \times 30$ and $144^3 \times 36$, but now applying the blocking method. The bin size is $4^3, 4^3, 4^3, 6^3, 8^3$ for each lattice respectively. The number of configurations is 10000 for all lattices. Other details

about the lattice setup and gradient flow setup can be found in [8].

In Fig. 5 we show a comparison of the correlators measured in the conventional way to those from the blocking method on the same configurations. Only correlators in the flow time range valid for the $\tau_F \rightarrow 0$ extrapolation are shown. In the left panel we take the finest available lattice as an example. In the right panel we compare the correlators after continuum extrapolation and flow time extrapolation. We find that the two ways of calculating the correlators give consistent results but with significantly reduced statistical uncertainty at the cost of introducing tiny systematic uncertainty when using the blocking method. We also repeat the spectral analysis carried out in [8] with the updated correlators, and find that the same Ansätze we considered there can not describe our data well any more. All the fits have $\chi^2/\text{d.o.f.} > 10$. This indicates that more sophisticated and physically motivated Ansätze for the spectral function are needed. We leave this for future work.

V. CONCLUSION

In this paper we propose a novel blocking method to improve the signal-to-noise ratio of Euclidean two-point correlators calculated on the lattice. Taking the bulk channel energy-momentum tensor correlators as an example, we demonstrate a factor of $3 \sim 7$ improvement in the signal-to-noise ratio, with almost no additional cost in numerical effort. Equivalently, this is a factor $10 \sim 50$ reduction in computational cost to achieve a given precision goal. We then apply the blocking method to the topological charge density correlators that we studied in a previous publication, finding that the Ansätze for the spectral function which we previously considered no

longer give a good fit to the data. Our blocking method can be easily implemented on the lattice and be used to study various correlators. It is applied at the analysis level, and does not have to be integrated into the configuration-generating procedure. There is also no obstacle to using it on unquenched lattices.

Let us briefly address our choice of bin size. We chose to use bins somewhat smaller than the largest τ -difference to be considered, in order to get sufficiently differential information about $G(s)$. As the bin size is made smaller, the numerical cost to correlate all bins eventually becomes significant. For the bin sizes considered here, this was not yet a problem. Also, as we make the bin size smaller, we increase the *relative* error in each individual bin, which might affect our procedure for choosing s_0 . If the bins are chosen smaller than the gradient-flow radius, then data at neighboring s values also becomes correlated, and autocorrelations in $G(\tau, s)$ at nearby s values must be handled carefully. In the opposite direction, if the bins are too large then we get an insufficiently refined determination of the s dependence of the correlation function. It might be useful to investigate systematically how bin-size choice affects our procedure, but we leave this for future investigation.

ACKNOWLEDGMENTS

All authors acknowledge support by the Deutsche Forschungsgemeinschaft (DFG, German Research Foundation) through the CRC-TR 211 ‘Strong-interaction matter under extreme conditions’- project number 315477589 – TRR 211. The computations in this work were performed on the GPU cluster at Bielefeld University using SIMULATeQCD suite [25, 26]. We thank the Bielefeld HPC.NRW team for their support.

-
- [1] H. B. Meyer, *Eur. Phys. J. A* **47**, 86 (2011), [arXiv:1104.3708 \[hep-lat\]](#).
 - [2] N. Astrakhantsev, V. Braguta, and A. Kotov, *JHEP* **04**, 101 (2017), [arXiv:1701.02266 \[hep-lat\]](#).
 - [3] M. Kitazawa, T. Iritani, M. Asakawa, and T. Hatsuda, *Phys. Rev. D* **96**, 111502 (2017), [arXiv:1708.01415 \[hep-lat\]](#).
 - [4] Borsányi, Sz. and Fodor, Zoltan and Giordano, Matteo and Katz, Sandor D. and Pasztor, Attila and Ratti, Claudia and Schäfer, Andreas and Szabo, Kalman K. and Tóth, Balint C., *Phys. Rev. D* **98**, 014512 (2018), [arXiv:1802.07718 \[hep-lat\]](#).
 - [5] Y. Taniguchi, A. Baba, A. Suzuki, S. Ejiri, K. Kanaya, M. Kitazawa, T. Shimojo, H. Suzuki, and T. Umeda, *PoS LATTICE2018*, 166 (2019), [arXiv:1901.01666 \[hep-lat\]](#).
 - [6] E. Itou and Y. Nagai, *JHEP* **07**, 007 (2020), [arXiv:2004.02426 \[hep-lat\]](#).
 - [7] G. Aarts and A. Nikolaev, *Eur. Phys. J. A* **57**, 118 (2021), [arXiv:2008.12326 \[hep-lat\]](#).
 - [8] L. Altenkort, A. M. Eller, O. Kaczmarek, L. Mazur, G. D. Moore, and H.-T. Shu, *Phys. Rev. D* **103**, 114513 (2021), [arXiv:2012.08279 \[hep-lat\]](#).
 - [9] R. Narayanan and H. Neuberger, *JHEP* **03**, 064 (2006), [arXiv:hep-th/0601210 \[hep-th\]](#).
 - [10] M. Lüscher and P. Weisz, *Commun. Math. Phys.* **97**, 59 (1985), [Erratum: *Commun.Math.Phys.* 98, 433 (1985)].
 - [11] M. Lüscher and P. Weisz, *JHEP* **09**, 010 (2001), [arXiv:hep-lat/0108014 \[hep-lat\]](#).
 - [12] H. B. Meyer, *Phys. Rev. D* **76**, 101701 (2007), [arXiv:0704.1801 \[hep-lat\]](#).
 - [13] H. B. Meyer, *Phys. Rev. Lett.* **100**, 162001 (2008), [arXiv:0710.3717 \[hep-lat\]](#).
 - [14] A. Francis, O. Kaczmarek, M. Laine, T. Neuhaus, and H. Ohno, *Phys. Rev. D* **92**, 116003 (2015), [arXiv:1508.04543 \[hep-lat\]](#).
 - [15] N. Brambilla, V. Leino, P. Petreczky, and A. Vairo, *Phys. Rev. D* **102**, 074503 (2020), [arXiv:2007.10078 \[hep-lat\]](#).
 - [16] M. Cè, L. Giusti, and S. Schaefer, *Phys. Rev. D* **93**, 094507 (2016), [arXiv:1601.04587 \[hep-lat\]](#).
 - [17] L. Giusti, M. Cè, and S. Schaefer, *EPJ Web Conf.* **175**,

- 01003 (2018), [arXiv:1710.09212 \[hep-lat\]](#).
- [18] G. Parisi, *Phys. Rept.* **103**, 203 (1984).
- [19] G. Bali, S. Collins, and A. Schafer (QCDSF), *PoS LAT2009*, 149 (2009), [arXiv:0911.2407 \[hep-lat\]](#).
- [20] W. Sun, A. Alexandru, Y. Chen, T. Draper, Z. Liu, and Y.-B. Yang (χ QCD), *Chin. Phys. C* **42**, 063102 (2018), [arXiv:1507.02541 \[hep-ph\]](#).
- [21] T. Blum, N. Christ, M. Hayakawa, T. Izubuchi, L. Jin, and C. Lehner, *Phys. Rev. D* **93**, 014503 (2016), [arXiv:1510.07100 \[hep-lat\]](#).
- [22] M. Cè, L. Giusti, and S. Schaefer, *Phys. Rev. D* **95**, 034503 (2017), [arXiv:1609.02419 \[hep-lat\]](#).
- [23] E. Shintani, T. Blum, T. Izubuchi, and A. Soni, *Phys. Rev. D* **93**, 094503 (2016), [arXiv:1512.00566 \[hep-lat\]](#).
- [24] K.-F. Liu, J. Liang, and Y.-B. Yang, *Phys. Rev. D* **97**, 034507 (2018), [arXiv:1705.06358 \[hep-lat\]](#).
- [25] L. Altenkort, D. Bollweg, D. A. Clarke, O. Kaczmarek, L. Mazur, C. Schmidt, P. Scior, and H.-T. Shu, [arXiv:2111.10354 \[hep-lat\]](#).
- [26] L. Mazur, *Ph.D. thesis*, Bielefeld University (2021), [10.4119/unibi/2956493](#).